

## Performance Optimization of Cermet SOFC Anodes: An Evaluation of Nanostructured NiO

Ilya Burmistrov, Dmitrii Agarkov, Ilya Tartakovskii, Vladislav Kharton  
and Sergey Bredikhin

Institute of Solid State Physics, Russian Academy of Sciences  
Chernogolovka, Moscow Dist. 142432, Russia

The electrochemical performance of the Ni-containing cermet anodes, widely used for all types of SOFCs, is essentially governed by the triple phase boundary (TPB) formed by metal, solid electrolyte and gaseous phase. Although the TPB length and electrode surface area may be drastically increased using nanostructured components, information on the resultant effects in terms of the cermet properties and SOFC production technology is still scarce. The present work is centered on the appraisal of NiO morphologies and optimization of pre-treatment conditions for the powders used for anode screen-printing, with commercial nanocrystalline nickel (II) oxide as a model starting material. A series of NiO powders were prepared via annealing at various temperatures (300 – 1100°C) followed by chemical, structural and morphological characterization. The results of X-ray diffraction (XRD), scanning and transmission electron microscopy (SEM/TEM), thermogravimetry and Raman spectroscopy reveal core-shell structure of nanosized NiO grains, formed due to surface hydration and oxidation under ambient conditions. Thermally induced desorption, and likely oxidation of organic components of the screen-printing pastes by the hyperstoichiometric oxygen, lead to poor quality of the electrode layers, thus making it necessary to introduce an additional powder pre-annealing step. The optimum pre-treatment temperature enabling to remove the absorbates, simultaneously preserving submicron grain size in the electrodes, corresponds to approximately 700°C.

### Introduction

The SOFC technology is one of the most promising for future energy industry (1-3). The efficiency of single SOFC is strongly dependent on the electrode performance. Despite the well-known problems such as carbon deposition (4-6) and Ni coarsening (7-10) during long-term operation, the anode cermets of metallic Ni and stabilized zirconia are among the most common SOFC materials. The electrochemical performance of the composite SOFC electrodes is essentially governed by the triple phase boundary (TPB) formed by electronic conductor, solid electrolyte and gaseous phase (7,11,12). One important approach to optimize the anode morphology relates to decreasing particle size of the initial powders (13,14). On the other hand, a drastic reduction of the component particle size may lead to dramatic changes in the material properties and electrode

behavior. The tendencies to agglomeration, a presence of modified surface layers and fast rates of microstructural alterations under SOFC operating conditions are all expected to considerably affect the electrode preparation procedure and anode behavior.

The present work was centered on the analysis of key relationships between the morphology of initial NiO powders used to form Ni-containing cermets and overall quality of the composite SOFC anodes.

## Experimental

The commercial nickel (II) oxide nanopowder (99.8% purity, Sigma-Aldrich) was employed as a model starting material for these case studies. In the course of optimization of the pre-treatment conditions, a series of NiO samples were annealed in air at 300, 500, 700, 900, 1000 and 1100°C for 1 h. To form the functional anode layer composites, NiO powders were mixed with submicron 10Sc1CeSZ (10 mol.% scandia and 1 mol.% ceria stabilized zirconia, DKKK, Japan) powder. The NiO / 10Sc1CeSZ mass ratio in the functional electrode layers, sandwiched between solid electrolyte membrane and current-collecting layers, was 40/60. In order to prepare pastes for screen-printing, the powders were mixed with a commercial V-006A thinner (Heraeus, Germany). An Ekra Mat S45 instrument (Germany) was employed for deposition of the electrode pastes.

The crystal structure of powdered samples was analysed by X-ray diffraction (XRD) using a Siemens D-500-Braun instrument ( $\text{CuK}_\alpha$  radiation). The particle size, composition and morphological features were assessed by scanning and transmission electron microscopy (SEM/TEM), combined with energy-dispersive spectroscopic analysis (EDX). The SEM/EDX studies were performed using a Supra 50VP microscope (Carl Zeiss, Germany) equipped with an INCA Energy+ microanalysis system. A Jeol JEM 100 CX II instrument (Japan) was employed for TEM analysis of the starting NiO powder. High-resolution TEM studies were carried out using a Jeol JEM 2100 microscope (Japan). The overall quality of the deposited layers was examined by optical microscopy using Olympus BX51 (Japan) equipped with a 9.1MP TouPCam CCD camera. For thermogravimetric analysis (TGA), a Netzsch STA 409C Luxx instrument (Germany) was used. This analyser equipped with a quadrupole mass-spectrometer QMS 403C Aeolos, provides simultaneous measurements of the TGA and differential scanning calorimetry (DSC) signals coupled with the evolved gas analysis. The room-temperature Raman spectra were collected using a home-made setup based on a LOMO MDR-12 diffraction grating monochromator (Russia) and 512x512 CCD camera (Princeton Instruments, USA).

## Results and Discussion

XRD analysis showed that the starting NiO nanopowder is single-phase, with pseudo cubic lattice parameter of 4.178(2) Å (Fig.1). As expected, at atmospheric oxygen pressure this phase remains stable in the entire temperature range studied in this work. The average crystallite size in the starting powder, calculated by the Scherrer equation, is 13 nm. This estimation was confirmed by statistical analysis of the TEM images (Fig.2),

which showed the maximum fraction of the particles has a size in the range of 5-15 nm. Over 99.5% particles are smaller than 50 nm.

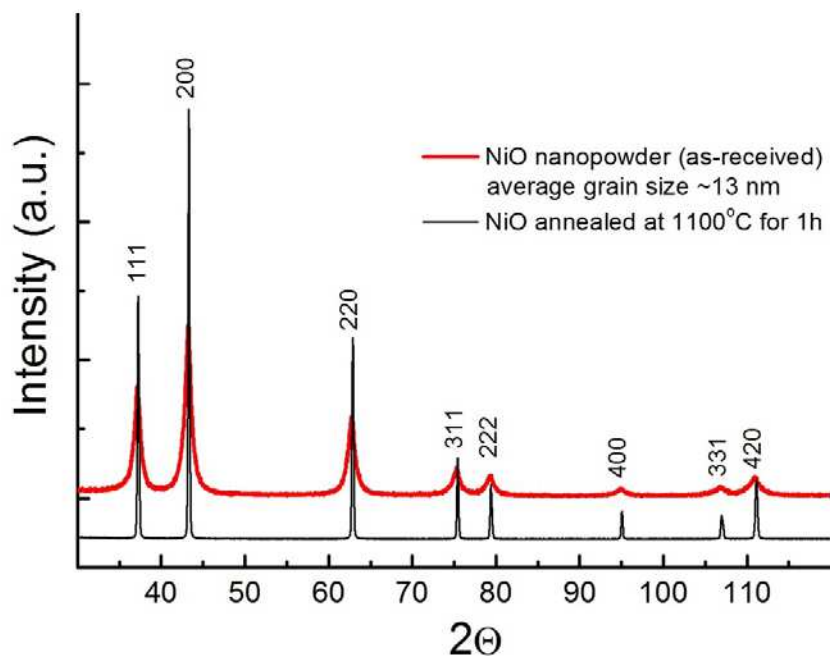


Figure 1. XRD patterns of starting NiO and the powder annealed at 1100°C for 1 h.

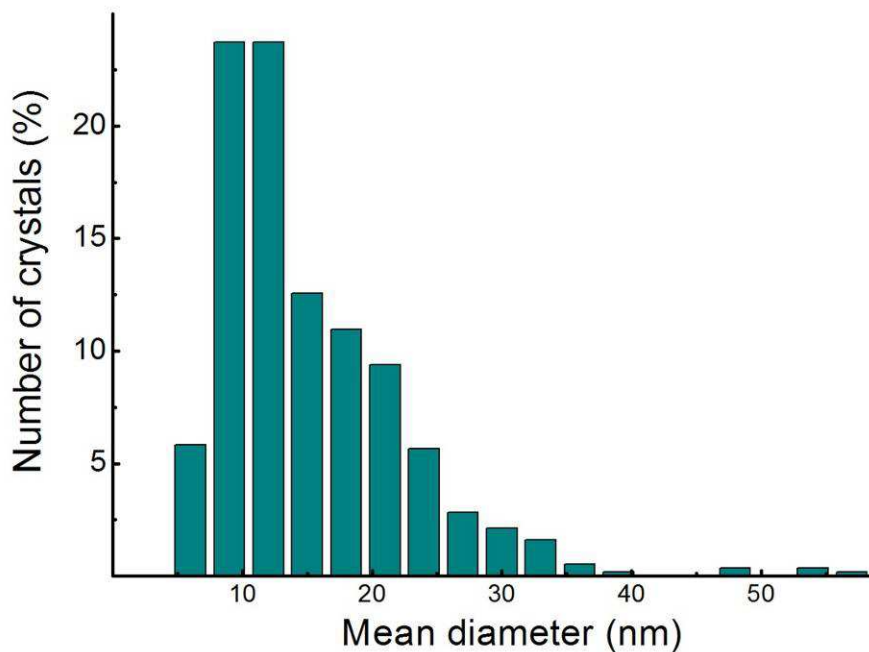


Figure 2. Particle size distribution in the starting NiO nanopowder, calculated from TEM results.

In theory, the use of such nanostructured powders for the anode preparation might be advantageous. However, after screen-printing and drying of the layers containing the starting NiO nanopowder, a strong tendency to cracking was observed; one example is presented in Fig.3. The defects formed during drying could not be eliminated by any subsequent sintering step. Due to very poor cohesion and large cracks, this kind of layers

cannot be used in practice. On the other hand, no similar behavior is observed for other NiO powders with micron and submicron particle size, used as a component of the screen-printing pastes; the screen-printing technology and NiO-containing pastes are worldwide used for the SOFC anode fabrication. The observed anomaly was, therefore, ascribed to specific morphological features of the NiO nanopowder. These features were assessed by high-resolution (HR) TEM in combination with TGA.

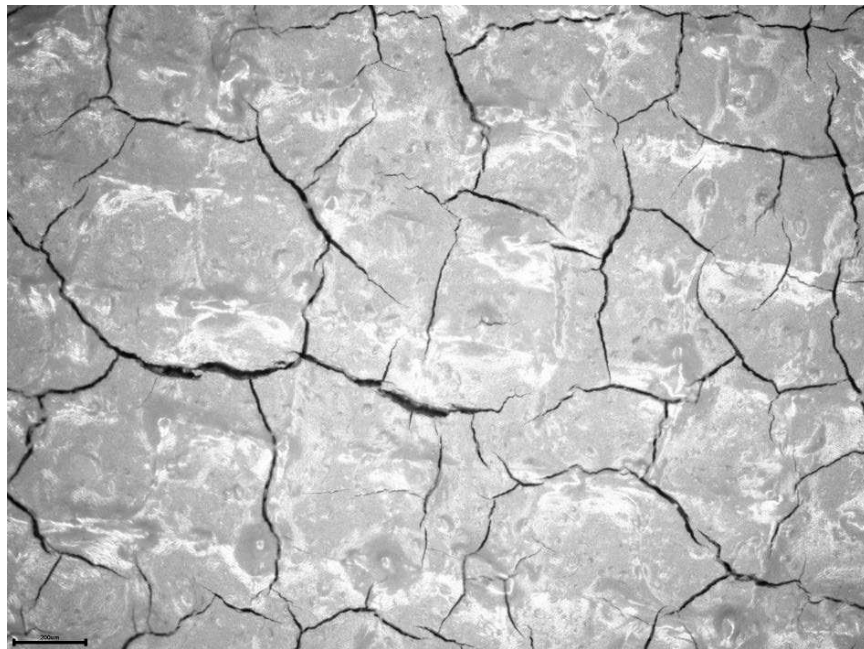


Figure 3. Photograph of the screen-printed functional anode layer after drying in air at 130°C.



Figure 4. HRTEM image of the starting NiO nanopowder.

HRTEM revealed a core-shell structure of NiO nanoparticles (Fig.4). The amorphous shell, up to 5 nm in thickness, was assumed formed due to absorption of gaseous species under ambient conditions. Indeed, EDX shows a substantially high oxygen

hyperstoichiometry of the nanopowder (Fig.5). The amount of extra oxygen decreases on annealing in air and becomes insignificant after heat-treatments at temperatures above 500°C.

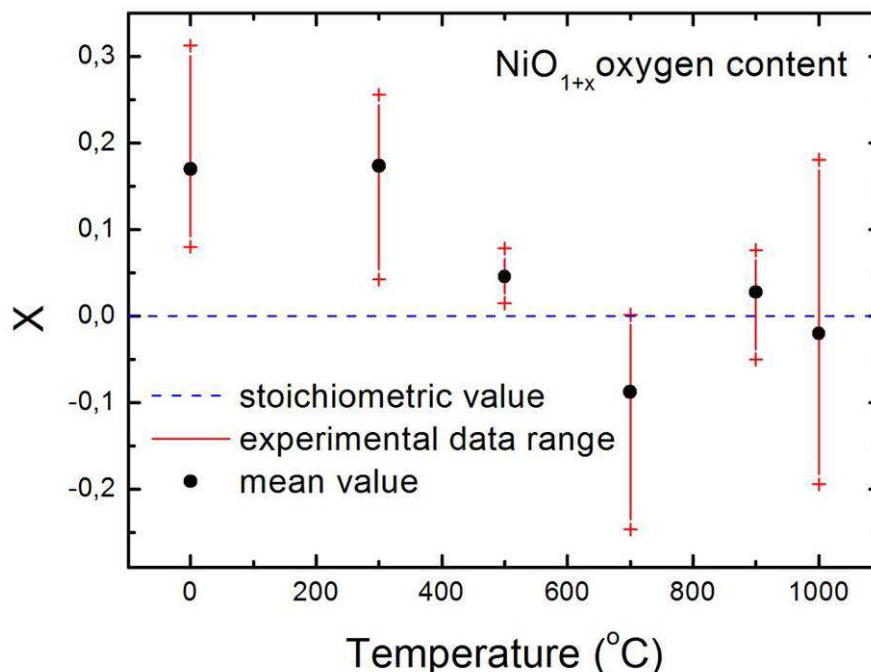


Figure 5. Oxygen content (x) in  $\text{NiO}_{1+x}$  powders annealed at different temperatures in air, as estimated by EDX.

In order to avoid uncertainties associated with EDX analysis of light elements, these observations were quantified by TGA. The starting NiO powder was studied in flowing air, argon and 4%  $\text{H}_2$  – 96% Ar mixture (4 vol. % of hydrogen); the mass-spectrometry signal was measured during heating in argon. The results are presented in Fig.6. The weight variations in air and argon atmospheres are equal within the limits of instrumental accuracy. This indicates that no organic adsorbates, which would burn in air, are present. There are two temperature ranges when extensive weight losses are observed. The mass-spectrometric data show that the first step in the thermogravimetric curves (60-200°C), with 3.6% weight loss, corresponds to dehydration. The calculated content of the desorbed water is  $0.16 \pm 0.03$  molecules per NiO formula unit. The second drop (300-600°C) is associated with the extra oxygen losses. The latter is clearly evidenced by the  $m/e=32$  peak detected by the mass-spectrometer. The total amount of desorbed oxygen corresponds to  $0.18 \pm 0.04$  atoms per formula unit. In the case of  $\text{H}_2$ -containing atmosphere, the hyperstoichiometric oxygen desorption is combined with total NiO reduction into metallic nickel, used as reference for the total oxygen content calculations from the TGA data.

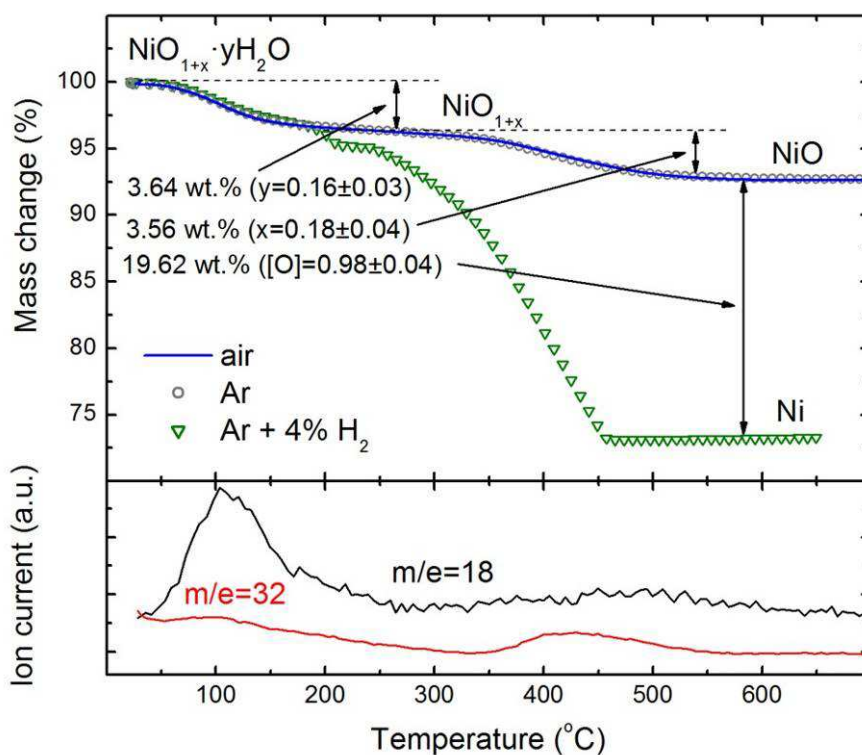


Figure 6. TGA curves of the starting NiO powder in various atmospheres (top) and strongest mass-spectrometric signals on heating in flowing argon (bottom).

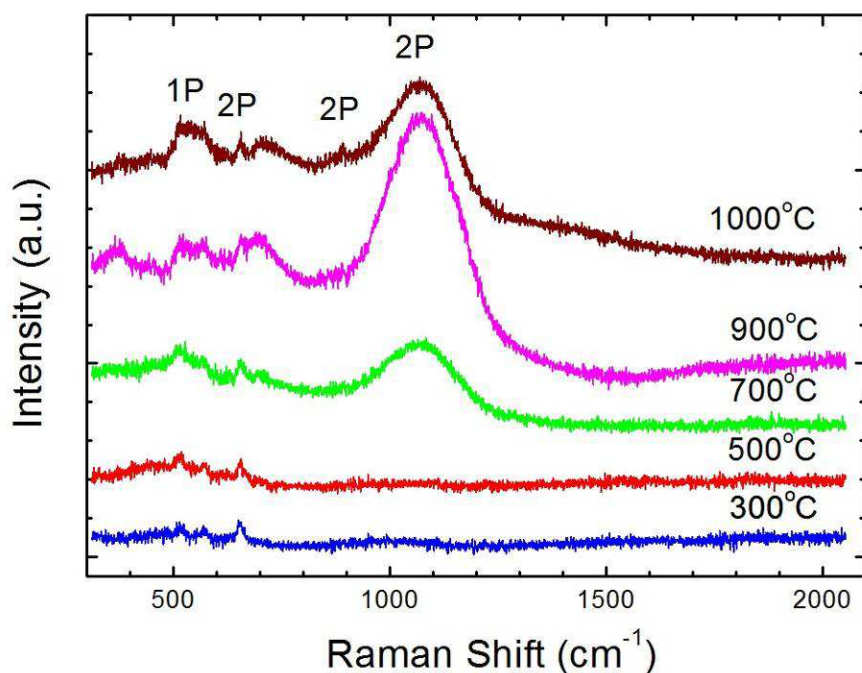


Figure 7. Raman spectra of NiO powders annealed at different temperatures.

The collected Raman spectra of the powders pre-annealed at various temperatures (Fig.7) are in excellent agreement with the HRTEM, EDX and TGA data. For annealing at 300-500°C, the characteristic peaks of NiO are almost invisible, confirming the presence of amorphous surface layers formed due to water and oxygen intercalation. For example, no strongest peak at  $\sim 1100 \text{ cm}^{-1}$  associated with two-phonon scattering can be

identified in these spectra. The first Raman spectrum with well-resolved NiO peaks was collected for the powder annealed at 700°C, when the absorbates are removed (Figs.5-6). Notice that thermal pre-treatment at 700°C makes it possible to preserve submicron size of the particles (Fig.8); the extensive grain growth starts on heating above 900°C. The former temperature was hence selected for the treatment of NiO powder introduced into the screen-printing paste for anode fabrication.

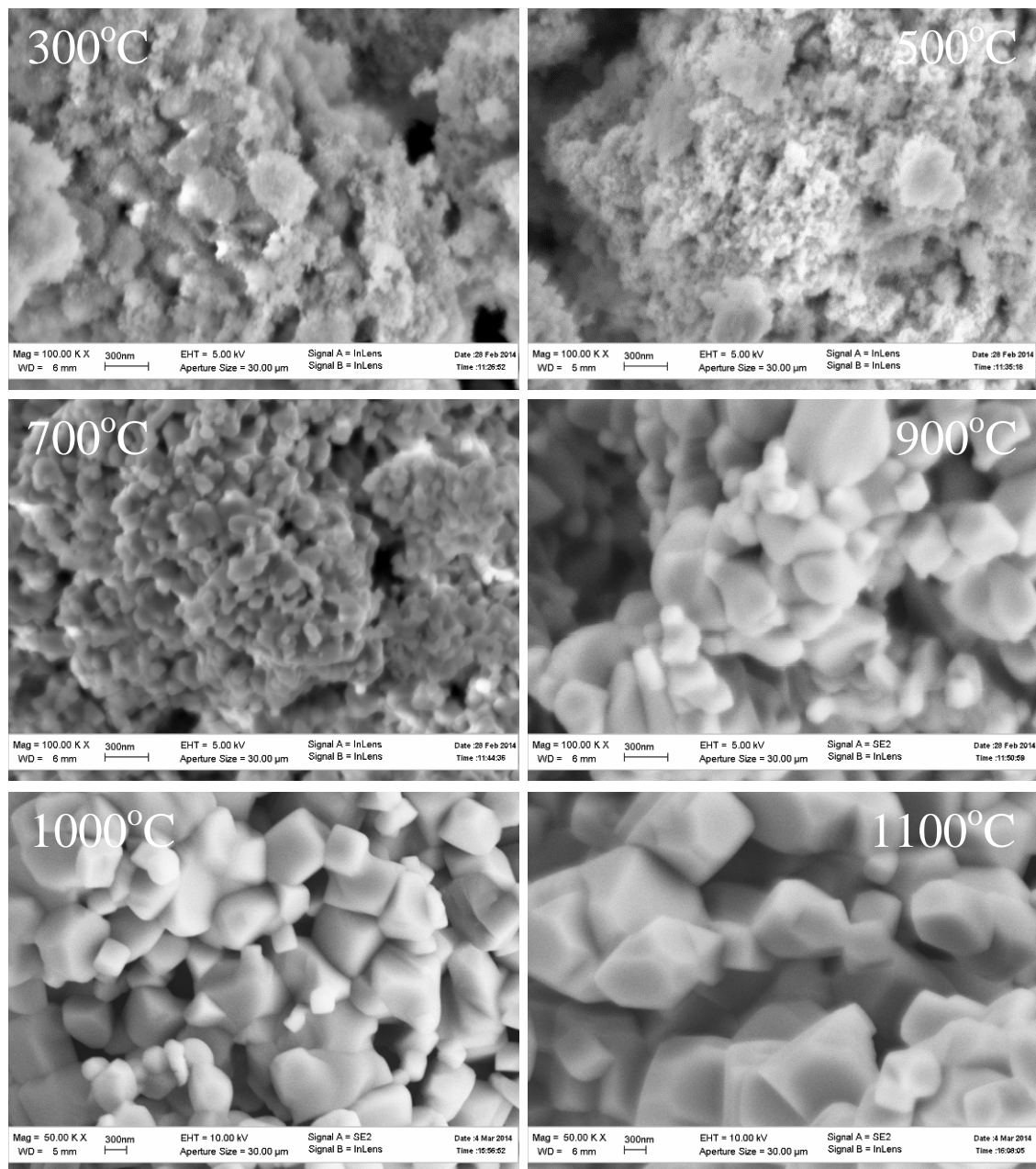


Figure 8. SEM images of the NiO powders pre-annealed at 300, 500, 700, 900, 1000 and 1100°C in air.

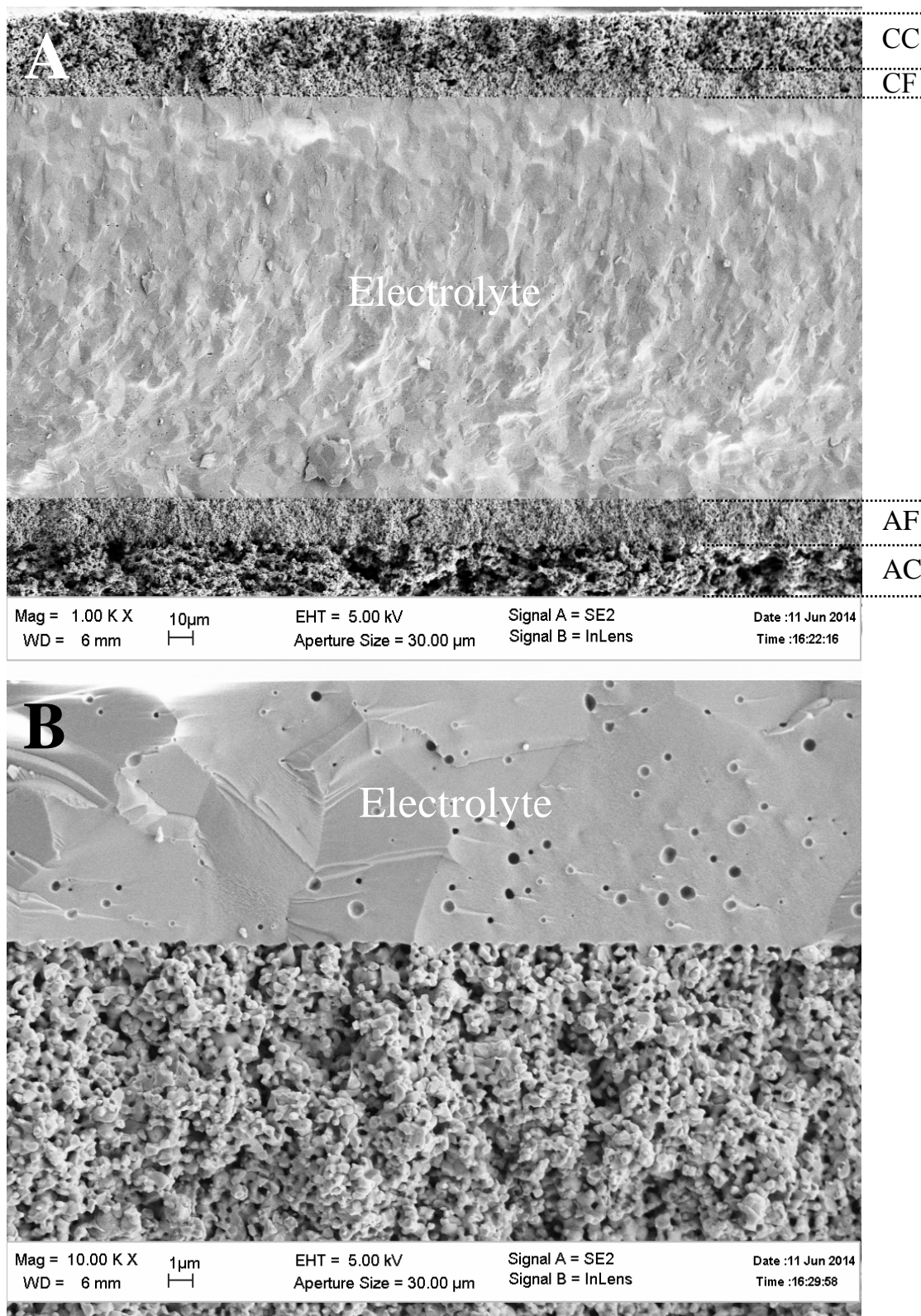


Figure 9. SEM micrographs of the model cell cross-section (A) and functional anode layer | electrolyte interface (B). The abbreviations CC, CF, AC and AF correspond to the cathode current-collecting, cathode functional, anode current-collecting and anode functional layers, respectively.

The experimental procedures and conditions, used for the model SOFC fabrication, were analogous to those reported elsewhere (16). The cell architecture comprising two-layer electrodes applied onto each side of the solid electrolyte membrane of stabilized zirconia, is illustrated by the cross-section shown in Fig.9(A). The SEM micrograph in Fig.9(B) displays typical microstructure of the anode function layer, prepared from the NiO powder pre-annealed at 700°C. This layer is placed between the solid electrolyte and current-collecting layer made of a similar cermet with the starting NiO/10Sc1CeSZ ratio of 60/40 in order to provide high electronic conductivity. The functional layer has a good adhesion to the other components of the planar cell and well-developed microstructure with an average particle size smaller than 1  $\mu\text{m}$ . The electrochemical behavior of the model SOFCs with such electrodes will be reported in forthcoming publications.

### Conclusions

Due to strong tendencies to absorption of extra oxygen and water vapour, the use of nanocrystalline NiO for composite anode screen-printing is associated with severe limitations. Drying of the screen-printed layers leads to cracking and poor cohesion originating from extensive desorption processes on heating. Most likely, these processes are accompanied with oxidation of organic components of the screen-printing paste by the hyperstoichiometric oxygen evolved from  $\text{NiO}_{1+x}$ . HRTEM, EDX, TGA and Raman spectroscopy studies revealed substantially large amounts of the extra oxygen, up to 20-30 at.%, which is incorporated into amorphous surface layers of the nanosized NiO particles. This behavior makes it necessary to introduce an additional heat-treatment step prior to the paste preparation. Annealing at temperatures above 500-600°C was shown to be enough for full elimination of the absorbates. Taking into account that extensive grain growth starts on heating above 900°C, the pre-treatment temperature of 700°C was selected as optimum.

### Acknowledgments

This work was supported by the Ministry of Education and Science of the Russian Federation (Russian Federation President grant 14.W01.15.5794-MK for support of young researchers).

### References

1. E. D. Wachsman, C. A. Marlowe, K. T. Lee, *Energ. Environ. Sci.*, **5** (2), 5498 (2012)
2. L. Blum, L. G. J. B. de Haart, J. Malzbender, N. H. Menzler, J. Rimmel, R. Steinberger-Wilckens, *J. Power Sources*, **241**, 477 (2013)
3. M. Liu, M. E. Lynch, K. Blinn, F. M. Alamgir, Y. Choi, *Mater. Today*, **14** (11), 534 (2011)
4. H. He, J. M. Hill, *Appl. Catal. A*, **317** (2), 284 (2007).
5. T. Chen, W. G. Wang, H. Miao, T. Li, C. Xu, *J. Power Sources*, **196** (5), 2461 (2011).

6. X.-M. Ge, S.-H. Chan, Q.-L. Liu, Q.-Sun, *Adv. Energy Mater.*, **2** (10), 1156 (2012).
7. G. J. Nelson, K. N. Grew, J. R. Izzo Jr., J. J. Lombardo, W. M. Harris, A. Faes, A. Hessler-Wyser, J. Van Herle, S. Wang, Y. S. Chu, A. V. Virkar, W. K. S. Chiu, *Acta Mater.*, **60** (8), 3491 (2012).
8. D. Simwonis, F. Tietz, D. Stöver, *Solid State Ionics*, **132** (3-4), 241 (2000).
9. M. H. Pihlatie, A. Kaiser, M. Mogensen, M. Chen, *Solid State Ionics*, **189** (1), 82 (2011).
10. J. Ayawanna, D. Wattanasiriwech, S. Wattanasiriwech, K. Sato, *Energy Procedia*, **34**, 439 (2013).
11. R. Ebrahim, M. Yeleuov, A. Issova, S. Tokmoldin, A. Ignatiev, *Nanoscale Res. Lett.*, **9**, 286 (2014).
12. P. S. Jørgensen, S. L. Ebbenhøj, A. Hauch, *J. Power Sources*, **279**, 686 (2015).
13. D. H. Prasad, H.-I. Ji, H.-R. Kim, J.-W. Son, B.-K. Kim, H.-W. Lee, J.-H. Lee, *Appl. Catal. B*, **101** (3-4), 531 (2011).
14. E. D. Wachsman, K. T. Lee, *Science*, **334**, 935 (2011).
15. O. V. Tiunova, O. Y. Zadorozhnaya, Y. K. Nepochatov, I. N. Burmistrov, I. E. Kuritsyna, S. I. Bredikhin, *Russ. J. Electrochem.*, **50** (7), 690 (2014).
16. I. Burmistrov, D. Agarkov, S. Bredikhin, Y. Nepochatov, O. Tiunova, O. Zadorozhnaya, *ECS Trans.*, **57** (1), 917 (2013).